American Mineralogist, Volume 67, pages 725–735, 1982

Thermodynamic mixing properties of corundum–eskolaite, α–$(Al,Cr^{+3})_2O_3$, crystalline solutions at high temperatures and pressures

NIRANJAN D. CHATTERJEE, HANS LEISTNER[1], LUDGER TERHART, KURT ABRAHAM, AND ROLF KLASKA

Institute of Mineralogy, Ruhr University, 4630 Bochum, Germany

Abstract

Corundum–eskolaite, α–$(Al,Cr)_2O_3$, crystalline solutions with compositions in the range $O < X_{Cr_2O_3} < 1$ have been synthesized at 25 kbar P_{H_2O} and 1070° C. Homogeneity of the crystals was checked and chemical compositions established by electron-probe microanalysis. Calculations of cell volumes based on 20 to 27 powder diffraction peaks, including those from the back reflection region, indicate a positive V_m^{ex} throughout the range of composition. Structure refinement of one synthetic crystal of $(Al_{0.49}Cr_{0.51})_2O_3$ composition confirmed a 1:1 Al–Cr statistical occupancy of the Al positions.

Information on H_m^{ex}, and S_m^{ex} of corundum–eskolaite crystalline solutions at 1 bar was obtained by reevaluating Jacob's (1978) *emf* data. By coupling these data with those for V_m^{ex}, a polybaric, polythermal equation of state was formulated. The G_m^{ex} can be expressed at any P and T as a function of $X_{Cr_2O_3}$:

$$G_m^{ex} = (1-X_{Cr_2O_3})\cdot X_{Cr_2O_3}\,[W_{G,Cr_2O_3} + (W_{G,Al_2O_3} - W_{G,Cr_2O_3})\cdot X_{Cr_2O_3}],$$

with $W_{G,Cr_2O_3} = 37484 + 0.0386\,P + 4.334\,T$, and
$W_{G,Al_2O_3} = 31729 + 0.0006\,P + 4.719\,T$,
P in bars, T in K and G_m^{ex} in joules.

Solvi for the Al_2O_3–Cr_2O_3 system have been computed using the G_m^{ex} expression given above. At a pressure of 1 bar, the critical temperature, T_c, was found to be 945° C, the critical composition, X_c, being 0.45 $X_{Cr_2O_3}$, whereas at 50 kbar T_c = 989° C and X_c = 0.44 $X_{Cr_2O_3}$. Thus, the pressure dependence of the solvus is very slight, and it may be regarded as an excellent geothermometer. Application of this geothermometer to exsolved chromian corundum and aluminous eskolaite from a grosspydite xenolith of the Zagadochnaya kimberlite pipe in Yakutia indicates reequilibration down to 910° C during the cooling episode.

Symbols and constants

T Temperature in Kelvin (K), unless otherwise specified (*e.g.*, Celsius, °C).

P Pressure in bar or kilobar (kbar).

emf Electromotive force (*emf*) of a galvanic cell.

$\bar{Y}_{m,i}$ Partial molar quantities of mixing for the ith component; Y : G, Gibbs energy (joule), S, entropy (joule·K^{-1}).

$\bar{Y}_{m,i}^{ex}$ Partial molar excess quantities of mixing for the ith component; Y : H, enthalpy (joule), C_p, heat capacity at constant pressure (joule·K^{-1}), S, and G.

Y_m^{ex} Integral molar excess quantities of mixing; Y : V, volume (joule·bar^{-1}), H, S, and G.

$W_{Y,i}$ Asymmetric Margules mixing parameter for the ith component (identical to $\bar{Y}_{m,i}^{ex,\infty}$, partial molar excess quantities of mixing of the ith component at infinite dilution); Y : U, internal energy (joule), S, H, G, and V.

a_i Activity of the ith component in a crystalline solution, referred to the standard state indicated in the text.

γ_i Activity coefficient of the ith component in a crystalline solution, as defined in equations (6) and (7).

X_i Mole fraction of the ith component.

R Gas constant, 8.3143 joules·K^{-1}·mol^{-1}.

F Faraday constant, 96 487 joules·volt^{-1}·mol^{-1}.

Introduction

Corundum–eskolaite, α–$(Al,Cr)_2O_3$, crystalline solutions are of interest in geochemistry and materi-

[1]Present address: Didier Forschungsinstitut, 6200 Wiesbaden, Germany.

0003–004X/82/0708–0725$02.00

al sciences alike. For this reason, numerous attempts have been made to determine the relationships between chemical composition, $X_{Cr_2O_3}$, and various physical properties such as optical absorption spectra, magnetic behavior, sound velocities, densities, and lattice parameters. While complete miscibility between the isostructural end-members corundum, α–Al_2O_3, and eskolaite, α–Cr_2O_3, has been demonstrated at high temperatures (Bunting, 1931), their natural analogues, with very few exceptions, show a limited range of composition. Corundum solid solutions in crustal rocks contain only a few mole percent of Cr_2O_3 component, while eskolaite contains little or no Al_2O_3 (Kouvo and Vuorelainen, 1958; Cassedanne and Cassedanne, 1980). These observations may reflect a scarcity of proper bulk compositions in nature and/or the presence of a wide miscibility gap under the conditions of rock formation. Knowledge of subsolidus phase relation in the system Al_2O_3–Cr_2O_3 is, therefore, of immediate interest.

Previous and present work

Earlier attempts to establish the miscibility gap in the system Al_2O_3–Cr_2O_3 yielded contradictory results. Thus, on a 2 kbar isobaric section, Neuhaus (1963) indicated a critical temperature, T_c, of 800° C and a critical composition, X_c, of 0.40 $X_{Cr_2O_3}$. By contrast, Roy and Barks (1972) found T_c = 945° C and X_c = 0.45 $X_{Cr_2O_3}$ at 1 kbar. Because synthesis runs of rather short duration served as the basis for both of these studies, discordant results are not surprising. Indeed, the possibility of a direct reversible determination of the solvus on this join seems to be remote due to notoriously slow ion diffusivity (Freer, 1981). Also noteworthy is the disparity in the nature and magnitude of the V_m^{ex} data supplied by various authors (Thilo *et al.*, 1955; Graham, 1960; Neuhaus, 1963; v. Steinwehr, 1967; Roy and Barks, 1972). Much of this confusion appears to stem from the difficult task of preparing homogeneous synthetic material of well known composition.

The purpose of the present study is threefold. First, V_m^{ex} data are reported for demonstrably homogeneous and microprobe–analyzed α–$(Al,Cr)_2O_3$ crystalline solutions. Second, electrochemically determined activities, $a_{Cr_2O_3}$ (Jacob, 1978) and $a_{Al_2O_3}$, are combined with V_m^{ex} data to formulate an equation of state for this crystalline solution series. Finally, solvi calculated from this equation are applied to pertinent geologic occurrences.

Synthesis and characterization of phases on the join Al_2O_3–Cr_2O_3

Experimental techniques

Starting materials were hydroxide gels of prescribed compositions prepared from Al metal (99.99%, E. Merck, Darmstadt, Lot No. 1057) and $Cr(NO_3)_3 \cdot 9H_2O$ (E. Merck, Darmstadt, Lot No. 2481) dissolved in an aqueous solution of HNO_3 and precipitated with excess NH_4OH. The coprecipitated hydroxides were subsequently fired at 500° C to decompose NH_4NO_3; the low temperature chosen for this purpose was to guard against loss of chromium. In all, nine gels were prepared at intervals of 0.1 $X_{Cr_2O_3}$.

The gels were welded shut in gold tubes with ~10 wt.% deionized H_2O and run at 900° C, 3 kbar P_{H_2O} for one day in an internally heated pressure vessel. Judging by the sharpness of the X-ray diffraction peaks, only the compositions 0.1 and 0.9 $X_{Cr_2O_3}$ yielded homogeneous phases. Grinding the products and repeating the runs twice more under identical conditions did not improve the sharpness of the X-ray diffraction peaks for intermediate compositions. The products of syntheses were reddish–pink in the range $0.1 \leq X_{Cr_2O_3} \leq 0.2$, and greenish for all compositions with $X_{Cr_2O_3} \geq 0.3$.

Homogeneous synthetic phases, as demonstrated by electron probe microanalyses, were eventually obtained by rerunning the charges at 25 kbar and 1070±30°C for two days in a 3/4″ solid-media apparatus using NaCl as a pressure medium. The X-ray diffraction peaks were generally very sharp, showing clear α_1/α_2 splits for Cu$K\alpha$–radiation above 40° 2θ, the sole exception being the charge with $X_{Cr_2O_3}$ = 0.4. Another noteworthy feature of the 25 kbar run products was that the red-green color transition was now at $X_{Cr_2O_3} \simeq 0.45$, rather than at $\simeq 0.25$ observed earlier in the inhomogeneous material prepared at 3 kbar.

The lattice constants of the synthetic materials were refined by standard powder X-ray diffraction techniques. Two scans in the range $40° \leq 2\theta$ Cu$K\alpha \leq 140°$ were obtained for each material at 0.25 2θ/min. and a 1 sec. time constant. Silicon (NBS standard reference material 640, with a = 5.43088Å) was used as an internal standard. Peak positions were measured near the top of the α_1 split, averaged, and then used for refinements of the lattice constants. In all cases, except for the material with $X_{Cr_2O_3}$ = 0.4, between 20 and 27 X-ray diffraction peaks could be processed. The least–squares refine-

ments of the cell dimensions involved the computer program by Appleman and Evans (1973), with $\lambda_{CuK\alpha_1} = 1.54050$Å.

The synthetic phases were analyzed with an electron probe microanalyzer (Microscan Mk V, Cambridge Scientific Instruments Ltd., U.K.), following the technique described by Abraham and Schreyer (1973). Synthetic Al_2O_3 and Cr_2O_3 single crystals served as standards. In recasting the analytical data to structural formulae, it was assumed that all chromium was in the trivalent state, a reasonable assumption in view of the large field of stability for Cr^{+3} in oxides and silicates (Navrotsky, 1975).

Phases synthesized

All data characterizing the synthetic phases are listed in Table 1. The results of the microprobe work deserve comment. First, the measured composition of the synthetic $(Al,Cr)_2O_3$ crystalline solutions closely match the nominal bulk compositions of the starting materials. Second, the standard deviations of the mean, σ, calculated from the formula

$$\sigma = \left[\sum_i (x_i - \bar{x})^2/n(n-1)\right]^{1/2}$$

are extremely small, indicating a high degree of homogeneity achieved during the synthesis. The sole exception to this is the material prepared from the bulk composition $X_{Cr_2O_3} \simeq 0.4$; in this case, σ is an order of magnitude higher. A closer look at this material revealed a two-phase assemblage, ~70% of which had the composition 0.40 $X_{Cr_2O_3}$, the rest 0.47. For this reason no more than 15 X-ray diffraction peaks were amenable to processing for the refinement of cell dimensions.

Excess molar volumes of mixing

The molar value data, V, listed in Table 1, have been fitted to a third-order polynomial in $X_{Cr_2O_3}$ by the method of least squares:

$$V = 2.5574(1) + 0.3867(102)\, X_{Cr_2O_3} - 0.0767(277)\, X^2_{Cr_2O_3} + 0.0380(178)\, X^3_{Cr_2O_3} \text{ joules·bar}^{-1} \quad (1)$$

Utilizing these data and following Waldbaum and Thompson (1968), we obtain

$$W_{V,Cr_2O_3} = 0.0386(102) \text{ joule·bar}^{-1} \quad (2a)$$

and

$$W_{V,Al_2O_3} = 0.0006(90) \text{ joule·bar}^{-1} \quad (2b)$$

Thus, V^{ex}_m can be expressed in terms of an asymmetric (two-parameter) Margules-type relation,

$$V^{ex}_m = (1-X_{Cr_2O_3})\cdot X_{Cr_2O_3}\,[W_{V,Cr_2O_3} + (W_{V,Al_2O_3} - W_{V,Cr_2O_3})\cdot X_{Cr_2O_3}] \quad (3)$$

We wish to stress that these data were obtained from volume measurements on composition-controlled, homogeneous synthetic materials.

Crystal structure refinement

We have also performed a structure refinement for a synthetic crystal of α-$(Al_{0.49}Cr_{0.51})_2O_3$. A crystal with an average diameter of 40 μm was chosen for X-ray study. Rotation, Weissenberg and precession photographs gave preliminary informa-

Table 1. Properties of synthetic α-$(Al,Cr)_2O_3$ crystalline solutions prepared at 1070±30° C, 25 kbar, 2 days

Nominal composition of starting material $X_{Cr_2O_3}$	Number of lines used in cell dimensions refinements	Cell dimensions a(Å)	c(Å)	V(Å^3)	Phase compositions from microprobe analyses	Molar Volumes V(joule.bar^{-1})
0.0	26	4.7592(1)	12.9918(4)	254.835(10)[1]		2.5577(1)
0.1	26	4.7840(1)	13.0538(4)	258.727(10)	0.1047(6)	2.5968(1)
0.2	22	4.8070(1)	13.1166(4)	262.486(10)	0.1997(19)	2.6345(1)
0.3	20	4.8282(1)	13.1763(4)	266.005(10)	0.3117(12)	2.6698(1)
0.4	15	4.8489(1)	13.2373(6)	269.532(15)	0.4039(32) and 0.4700(15)	2.7052(2)[2]
0.5	24	4.8696(1)	13.2980(4)	273.084(11)	0.5107(22)	2.7409(1)[3]
0.6	25	4.8891(1)	13.3565(3)	276.490(9)	0.6218(15)	2.7751(1)
0.7	23	4.9089(1)	13.4213(4)	280.083(11)	0.7241(9)	2.8111(1)
0.8	26	4.9255(1)	13.4749(3)	283.114(9)	0.8072(17)	2.8416(1)
0.9	27	4.9428(1)	13.5337(3)	286.352(9)	0.9064(14)	2.8741(1)
1.0	26	4.9585(1)	13.5952(2)	289.479(7)		2.9054(1)

1) *All quantities in parentheses denote one standard deviation.*
2) *Two-phase assemblage (see text for further comments). Molar volume ignored while deriving equation(1).*
3) *Crystal structure refinement was performed on this material.*

tion on the space group symmetry $R\bar{3}c$ and lattice constants.

For data collection on a four-circle Syntex R3 diffractometer, optimized angular settings were derived on the basis of 25 high-index *hkl* reflections. The integral intensities were measured by the $\omega/2\theta$ scan technique, using graphite monochromatized Mo$K\alpha$–radiation. These data were converted to corrected $|F|$–values through Lorentz-polarization corrected data reduction. Spherical absorption correction was ignored. Of the 163 symmetrically independent reflections recorded in the range $\sin\theta/\lambda = 0.808$, 151 reflections sufficed to meet the criterion $I_{net} > 1.96\sigma$, σ being the standard deviation of a Poisson distribution.

The initial atomic parameters for the structure refinement in the hexagonal setting were those listed by Moss and Newham (1964). Cr and Al are positioned on the $\bar{3}$ axis, while O prefers the diad. The preliminary X-ray investigation suggested the lack of any ordering of Cr, because neither a symmetry reduction nor additional reflections could be detected. The structure refinement confirmed an occupancy of the Al positions by Cr and Al in a 1:1 ratio. The difference Fourier synthesis based on the final cycle of refinement (Table 2) revealed no interpretable electron densities in the vicinity of the $\bar{3}$ axis. The final refinement converged to an unweighted R factor of 0.036, where $R = \Sigma|(|F_o| - |F_c|)/\Sigma|F_o|$.

Thermodynamics of α–$(Al,Cr)_2O_3$ crystalline solutions

Some relevant relations

For the purpose of thermodynamic treatment of $(Al,Cr)_2O_3$ crystalline solutions, the standard state chosen is one of unit activity of the pure component (with corundum structure) at system P and T. The integral molar Gibbs energy of mixing, G_m, of such a solution is expressed as

$$G_m = RT\,[(1 - X_{Cr_2O_3})\,ln\,a_{Al_2O_3} + X_{Cr_2O_3}\,ln\,a_{Cr_2O_3}] \quad (4)$$

Table 2. Final occupancies, positional parameters, and temperature factors of the atoms in synthetic α-$(Al_{0.49}Cr_{0.51})_2O_3$

Atoms	Occupancy	X	Y	Z	B(Å^2)
Cr	0.166(1)	0	0	0.3492(1)	0.83
Al	0.167(1)	0	0	0.3501(2)	0.83
O	0.515(3)	0.3056(5)	0	0.25	1.03

Recalling that Al and Cr mix on *two* symmetrically equivalent structural sites per formula unit, we may split G_m into an ideal, G_m^{id}, and an excess, G_m^{ex}, mixing term, such that

$$G_m^{id} = 2\,RT\,[(1 - X_{Cr_2O_3})ln(1 - X_{Cr_2O_3}) + X_{Cr_2O_3}\,ln\,X_{Cr_2O_3}] \quad (5a)$$

and $$G_m^{ex} = 2\,RT\,[(1 - X_{Cr_2O_3})ln\,\gamma_{AlO_{1.5}} + X_{Cr_2O_3}\,ln\,\gamma_{CrO_{1.5}}]. \quad (5b)$$

From the relations (4), (5a), and (5b) it is evident that for $(Al,Cr)_2O_3$ crystalline solutions

$$a_{Al_2O_3} = [(1 - X_{Cr_2O_3})\cdot\gamma_{AlO_{1.5}}]^2 = (a_{AlO_{1.5}})^2 \quad (6a)$$

and $$a_{Cr_2O_3} = (X_{Cr_2O_3}\cdot\gamma_{CrO_{1.5}})^2 = (a_{CrO_{1.5}})^2. \quad (6b)$$

However, if we choose Al_2O_3 and Cr_2O_3 as the mixing entities, rather than $AlO_{1.5}$ and $CrO_{1.5}$, as implied by (5b) and (6a,6b), G_m^{ex} must be rewritten as

$$G_m^{ex} = RT\,[(1 - X_{Cr_2O_3})ln\,\gamma_{Al_2O_3} + X_{Cr_2O_3}\,ln\,\gamma_{Cr_2O_3}]. \quad (5b')$$

Therefore, the activities must also be redefined as

$$a_{Al_2O_3} = (1 - X_{Cr_2O_3})^2\cdot\gamma_{Al_2O_3} \quad (7a)$$

and $$a_{Cr_2O_3} = X_{Cr_2O_3}^2\cdot\gamma_{Cr_2O_3}. \quad (7b)$$

In the following, we shall adopt Al_2O_3 and Cr_2O_3 as the mixing entities, to make our results directly comparable to those of Jacob (1978).

Another relevant problem concerning crystalline solutions such as $(Al,Cr)_2O_3$ is how best to describe the functional relationship between Y_m^{ex} and $X_{Cr_2O_3}$ at any P and T. Where direct information is lacking, the available data is commonly tested against some assumed linear relationship, *e.g.*, a Margules equation. *We stress that no such assumption is involved in our evaluation of the 1 bar Y_m^{ex} data.* $\overline{Y}_{m,Cr_2O_3}^{ex}$ is obtained from Jacob's (1978) *emf* measurements, $\overline{Y}_{m,Al_2O_3}^{ex}$ by Gibbs-Duhem integration. Knowledge of the two quantities permit direct evaluation of Y_m^{ex} *versus* $X_{Cr_2O_3}$. In every case, the equation

$$Y_m^{ex} = (1 - X_{Cr_2O_3})\cdot X_{Cr_2O_3}\,[W_{Y,Cr_2O_3} + (W_{Y,Al_2O_3} - W_{Y,Cr_2O_3})\cdot X_{Cr_2O_3}] \quad (8)$$

is found to adequately satisfy our Y_m^{ex} data. Thus, *the available data are not forced to meet the requirements of a Margules relation;* rather, $(Al,Cr)_2O_3$ *crystalline solutions are demonstrated to behave in a manner best described by* equation (8), *the asymmetric Margules relation.*

EMF data by Jacob (1978)

Recently, Jacob has measured the reversible electromotive force *(emf)* of the solid oxide galvanic cell

$$\text{Pt, Cr} + \text{Cr}_2\text{O}_3/\text{Y}_2\text{O}_3 - \text{ThO}_2/\text{Cr} + (\text{Cr,Al})_2\text{O}_3, \text{Pt}$$

in the temperature range 800–1320° C for seven discrete compositions spanning the range $0.1 \leq X_{Cr_2O_3} \leq 0.9$. For each composition, the *emf* was found to be linearly dependent on temperature. The measured *emf*, E, is related to $\overline{G}_{m,Cr_2O_3}$, $\overline{H}^{ex}_{m,Cr_2O_3}$, and $\overline{S}_{m,Cr_2O_3}$ by the relations:

$$\overline{G}_{m,Cr_2O_3} = RT\ ln\ a_{Cr_2O_3} = -6\ F\ E, \quad (9)$$

$$\overline{H}^{ex}_{m,Cr_2O_3} = -6\ F\ [E - T(\partial E/\partial T)_P], \quad (10)$$

$$\text{and } \overline{S}_{m,Cr_2O_3} = 6\ F\ (\partial E/\partial T)_P. \quad (11)$$

From the linear dependence of E on T it is immediately apparent that $\overline{H}^{ex}_{m,Cr_2O_3}$ is itself independent of T, at least for the range of temperature studied. In other words, $\overline{C}^{ex}_{p,m,Cr_2O_3} = 0$ and, consequently, $\overline{S}^{ex}_{m,Cr_2O_3}$ is also temperature-independent.

Using his *emf* data, Jacob (1978) evaluated G^{ex}_m, H^{ex}_m, and S^{ex}_m, for $(Al,Cr)_2O_3$ crystalline solutions. His final results were summarized as:

$$H^{ex}_m = X_{Cr_2O_3}X_{Al_2O_3}[W_{H,Al_2O_3}X_{Cr_2O_3} + W_{H,Cr_2O_3}X_{Al_2O_3}],$$

with $W_{H,Al_2O_3} = 31700$ joules
and $W_{H,Cr_2O_3} = 37470$ joules, and

$$S^{ex}_m = 0.2\ R\ [X_{Cr_2O_3}\ ln\ X_{Cr_2O_3} + X_{Al_2O_3}\ ln\ X_{Al_2O_3}].$$

Thus, he found that H^{ex}_m can be expressed in terms of an asymmetric Margules relation analogous to equation (8), but not S^{ex}_m or G^{ex}_m. This precluded our combining Jacob's (1978) results in a straightforward manner with our V^{ex}_m data to obtain a polybaric, polythermal equation of state for $(Al,Cr)_2O_3$ crystalline solutions. This situation, coupled with the fact that the format of the integrated Gibbs-Duhem equation employed by Jacob (1978),

$$\overline{Y}^{ex}_{m,Al_2O_3} = -\int_{X_{Cr_2O_3}=0}^{X_{Cr_2O_3}} (X_{Cr_2O_3})/(1 - X_{Cr_2O_3})\ d\overline{Y}^{ex}_{m,Cr_2O_3} \quad (12)$$

might lead to inaccurate results (see below), prompted our attempt to reevaluate Jacob's original *emf* data.

Reevaluation of Jacob's emf data

The first step in the reevaluation of Jacob's (1978) data is to derive $\overline{G}^{ex}_{m,Cr_2O_3}$ $(= RT\ ln\ \gamma_{Cr_2O_3})$ at a given T and $X_{Cr_2O_3}$ by combining the available *emf* data (Jacob, 1978, Table 1) with equations (9) and (7b). Next, $\overline{G}^{ex}_{m,Al_2O_3}$ is obtained by integrating the Gibbs-Duhem equation.

For binary $(Al,Cr)_2O_3$ crystalline solutions at any P and T, the Gibbs-Duhem relation is given by

$$(1 - X_{Cr_2O_3})\ d\overline{Y}^{ex}_{m,Al_2O_3} + X_{Cr_2O_3}\ d\overline{Y}^{ex}_{m,Cr_2O_3} = 0. \quad (13)$$

Straightforward integration, using the format of equation (12), can be executed graphically by plotting $X_{Cr_2O_3}/(1 - X_{Cr_2O_3})$ *vs.* $\overline{Y}^{ex}_{m,Cr_2O_3}$ and determining the area under the curve. Because $\overline{Y}^{ex}_{m,Cr_2O_3}$ has only been measured in the composition range $0.1 \leqq X_{Cr_2O_3} \leqq 0.9$, such an integration requires that $\overline{Y}^{ex}_{m,Cr_2O_3}$ be extrapolated to $X_{Cr_2O_3} = 0$, the lower limit of integration. In practice, this approach can introduce substantial error, regardless of how the extrapolation is accomplished. An additional problem arises when extrapolation of $\overline{Y}^{ex}_{m,Cr_2O_3}$ to $X_{Cr_2O_3} \rightarrow 1$ is attempted, because $X_{Cr_2O_3}/(1 - X_{Cr_2O_3})$ becomes undefined when $X_{Cr_2O_3} = 1$. This makes it very difficult to determine the area under the curve "with any accuracy" (Denbigh, 1971, p. 285).

To circumvent these problems, our integration follows a method devised by Chiotti (1972). This approach makes use of the fact that the product $X_{Cr_2O_3}\cdot\overline{Y}^{ex}_{m,Cr_2O_3}$ is zero both at $X_{Cr_2O_3} = 0$ and $X_{Cr_2O_3} = 1$. Introduction of these boundary constraints thus leads to a more reliable extrapolation of $\overline{Y}^{ex}_{m,Cr_2O_3}$ to $X_{Cr_2O_3} = 0$ and $X_{Cr_2O_3} = 1$. Following Chiotti, this goal is achieved by beginning with the derivative of $X^2_{Cr_2O_3}\ \overline{Y}^{ex}_{m,Cr_2O_3}$:

$$d\ (X^2_{Cr_2O_3}\overline{Y}^{ex}_{m,Cr_2O_3}) = 2\ X_{Cr_2O_3}\overline{Y}^{ex}_{m,Cr_2O_3}\ dX_{Cr_2O_3} + X^2_{Cr_2O_3}\ d\overline{Y}^{ex}_{m,Cr_2O_3}. \quad (14)$$

Substituting $-(1 - X_{Cr_2O_3})\ d\overline{Y}^{ex}_{m,Al_2O_3}$ for $X_{Cr_2O_3}\ d\overline{Y}^{ex}_{m,Cr_2O_3}$ (from equation 13) into (14) and rearranging,

$$-d(X^2_{Cr_2O_3}\ Y^{ex}_{m,Cr_2O_3}) + 2\ X_{Cr_2O_3}\overline{Y}^{ex}_{m,Cr_2O_3}\ dX_{Cr_2O_3} = X_{Cr_2O_3}\ (1 - X_{Cr_2O_3})\ dY^{ex}_{m,Al_2O_3}. \quad (15)$$

Integration of (15) between the limits $X_{Cr_2O_3} = 0$ and the desired value of $X_{Cr_2O_3}$ yields

$$-X^2_{Cr_2O_3}\overline{Y}^{ex}_{m,Cr_2O_3} + 2\int_{X_{Cr_2O_3}=0}^{X_{Cr_2O_3}} X_{Cr_2O_3}\overline{Y}^{ex}_{m,Cr_2O_3}\ dX_{Cr_2O_3} = \int_{X_{Cr_2O_3}=0}^{X_{Cr_2O_3}} X_{Cr_2O_3}\ (1 - X_{Cr_2O_3})d\overline{Y}^{ex}_{m,Al_2O_3}. \quad (16)$$

Evaluation of the integral on the left hand side of (16) is now straightforward, given the boundary constraints $X_{Cr_2O_3}\overline{Y}^{ex}_{m,Cr_2O_3} = 0$ both at $X_{Cr_2O_3} = 0$ and $X_{Cr_2O_3} = 1$. Additional control on the quantity $X_{Cr_2O_3}\overline{Y}^{ex}_{m,Cr_2O_3}$ as a function of $X_{Cr_2O_3}$ is established by the relations (Chiotti, 1972, p. 2913):

$$d(X_{Cr_2O_3}\overline{Y}^{ex}_{m,Cr_2O_3})/dX_{Cr_2O_3} = \overline{Y}^{ex,\infty}_{m,Cr_2O_3}, \text{ as } X_{Cr_2O_3} \rightarrow 0 \quad (17a)$$

$$\text{and } d(X_{Cr_2O_3}\overline{Y}^{ex}_{m,Cr_2O_3})/dX_{Cr_2O_3} = 0, \quad \text{as } X_{Cr_2O_3} \rightarrow 1. \quad (17b)$$

The value of $\overline{Y}^{ex,\infty}_{m,Cr_2O_3}$ was estimated by using plots of $\overline{Y}^{ex}_{m,Cr_2O_3}$ *vs.* $X_{Cr_2O_3}$ and $Y^{ex}_{m,Cr_2O_3}/(1 - X_{Cr_2O_3})^2$ *vs.* $X_{Cr_2O_3}$. At $X_{Cr_2O_3} = 0$, these two curves meet at a common intercept to yield the desired values of $\overline{Y}^{ex,\infty}_{m,Cr_2O_3}$ (Chiotti, 1972, p. 2913). The curve fitting through the uncertainty brackets of the measured data points and the four above mentioned boundary constraints for evaluation of the integral on the left hand side of (16) was accomplished by using an optimization routine. Note that evaluation of the left hand side of (16) gives the *integral* of the right hand side, from which $\overline{Y}^{ex}_{m,Al_2O_3}$ can be calculated utilizing the principle of the trapezoidal rule (Chiotti, 1972, p. 2912).

Details of curve fitting, data handling and two alternative approaches to verify the self-consistency of the derived G^{ex}_m, H^{ex}_m, and S^{ex}_m are given in the Appendix.

Results

Table 3 lists calculated values for $\overline{G}^{ex}_{m,Al_2O_3}$ at 1 bar, 1000° C based on Jacob's (1978) *emf* measurements and the present integration of the Gibbs-Duhem equation (equation 16). Also indicated are G^{ex}_m, calculated using (5b′), as well as G_m, obtained via equations (4) and (7). For comparison, G_m, as computed by Jacob (1978, Table 1), is reproduced. Note that the G^{ex}_m values of Jacob were derived from his G_m data.

Table 3 discloses substantial differences between values of G^{ex}_m and G_m obtained by us and those given by Jacob. Presumably, this is an outcome of different methods of integrating the Gibbs-Duhem equation, because both sets of data are based on identical *emf* measurements. This discrepancy becomes particularly conspicuous when the quantity $G^{ex}_m/(1 - X_{Cr_2O_3})\cdot X_{Cr_2O_3}$ is plotted against $X_{Cr_2O_3}$ (Fig. 1). Figure 1 shows that the present results can be expressed analytically in a linear form (asymmetric Margules equation) analogous to equation (8):

$$G^{ex}_m = (1 - X_{Cr_2O_3})\cdot X_{Cr_2O_3} [W_{G,Cr_2O_3} + (W_{G,Al_2O_3} - W_{G,Cr_2O_3}) X_{Cr_2O_3}], \quad (8a)$$

where $W_{G,Cr_2O_3} = 43002$ joules, (18a)

$W_{G,Al_2O_3} = 37737$ joules. (18b)

Note that these W_G values hold for 1 bar and 1000° C.

Table 4 lists the results of processing Jacob's (1978) *emf* measurements via equations (10) and (16), and Figure 2 shows that $H^{ex}_m/(1 - X_{Cr_2O_3})\cdot X_{Cr_2O_3}$ plotted against $X_{Cr_2O_3}$ obeys a linear relationship. Therefore, H^{ex}_m can also be represented by an asymmetric Margules equation:

$$H^{ex}_m = (1 - X_{Cr_2O_3})\cdot X_{Cr_2O_3} [W_{H,Cr_2O_3} + (W_{H,Al_2O_3} - W_{H,Cr_2O_3}) X_{Cr_2O_3}], \quad (8b)$$

with $W_{H,Cr_2O_3} = 37484$ joules, (19a)

$W_{H,Al_2O_3} = 31729$ joules. (19b)

Table 3. $\overline{G}^{ex}_{m,Al_2O_3}$, G^{ex}_m, $G^{ex}_m/(1 - X_{Cr_2O_3})\cdot X_{Cr_2O_3}$, and G_m values for corundum-eskolaite crystalline solutions at 1 bar, 1000° C

	This study				Jacob(1978)		
$X_{Cr_2O_3}$	$\overline{G}^{ex}_{m,Al_2O_3}$ (joules)	G^{ex}_m (joules)	$\frac{G^{ex}_m}{(1-X_{Cr_2O_3})X_{Cr_2O_3}}$ (joules)	G_m (joules)	G_m (joules)	G^{ex}_m (joules)	$\frac{G^{ex}_m}{(1-X_{Cr_2O_3})X_{Cr_2O_3}}$ (joules)
0.10	475	3824	42484	- 3058	- 2870	4012	44580
0.24	2636	7612	41734	- 4055	- 3920	7747	42471
0.37	6074	9568	41048	- 4383	- 4320	9631	41315
0.50	10748	10091	40365	- 4538	- 4560	10114	40485
0.64	17007	9131	39630	- 4702	- 4670	9163	39771
0.77	23808	6898	38949	- 4519	- 4430	6987	39451
0.90	31422	3444	38268	- 3438	- 3290	3592	39914

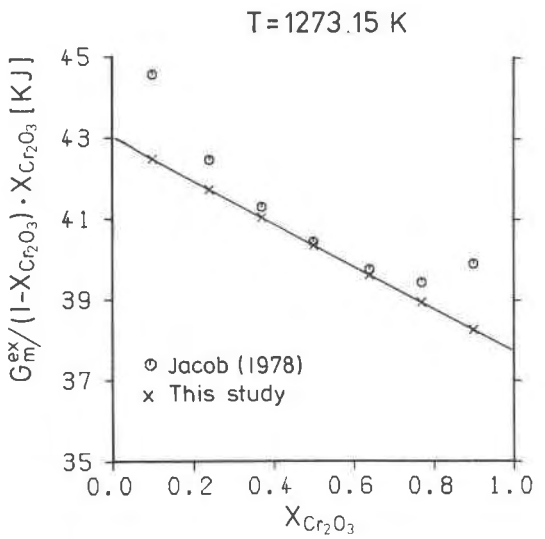

Fig. 1. $G_m^{ex}/(1 - X_{Cr_2O_3})\cdot X_{Cr_2O_3}$ *vs.* $X_{Cr_2O_3}$ diagram for T = 1273.15 K and P = 1 bar. The octagons show results obtained by Jacob (1978), the crosses are those obtained in this study for the seven discrete compositions subjected to *emf* measurements by Jacob. The bold line is based on 99 computations of the above quantity at intervals of 0.01 $X_{Cr_2O_3}$.

The present estimates of $W_{H,i}$ agree very well with those given by Jacob (1978, p. 177). Finally, combination of (18) and (19) yields

$$W_{S,Cr_2O_3} = -4.334 \text{ joules}\cdot K^{-1}, \quad (20a)$$

$$W_{S,Al_2O_3} = -4.719 \text{ joules}\cdot K^{-1}. \quad (20b)$$

As indicated earlier, both $W_{H,i}$ and $W_{S,i}$ are temperature-independent quantities.

The fact that mathematical expressions for all integral excess properties can be cast in a linear form such as equation (8) *proves* the validity of asymmetric Margules equations for $(Al,Cr)_2O_3$ crystalline solutions. Thus, from equations (2), (19) and (20), a polybaric, polythermal equation of state follows:

$$G_m^{ex} = (1 - X_{Cr_2O_3})\cdot X_{Cr_2O_3} [W_{G,Cr_2O_3} + (W_{G,Al_2O_3} - W_{G,Cr_2O_3}) X_{Cr_2O_3}] \quad (8a)$$

where $W_{G,Cr_2O_3} = 37484 + 0.0386\,P + 4.334\,T$, (21a)

and $W_{G,Al_2O_3} = 31729 + 0.0006\,P + 4.719\,T$. (21b)

Note that in equations (21a) and 21b),

$$W_{G,i} = W_{U,i} + P\,W_{V,i} + T\,W_{S,i}.$$

Because $W_{H,i} \equiv W_{U,i} + P\,W_{V,i}$, and $W_{V,i}$ is a negligible quantity compared to the uncertainties of $W_{H,i}$ at 1 bar, the numerical value of $W_{U,i}$ has been set identical to that of $W_{H,i}$ at 1 bar [compare equations (19) and (21)].

Table 4. $\bar{H}^{ex}_{m,Al_2O_3}$, H_m^{ex}, and $H_m^{ex}/(1 - X_{Cr_2O_3})\cdot X_{Cr_2O_3}$ obtained in this study using Jacob's (1978) *emf* measurements

$X_{Cr_2O_3}$	$\bar{H}^{ex}_{m,Al_2O_3}$ (joules)	H_m^{ex} (joules)	$\frac{H_m^{ex}}{(1-X_{Cr_2O_3})X_{Cr_2O_3}}$ (joules)
0.10	424	3322	36917
0.24	2333	6584	36099
0.37	5336	8240	35350
0.50	9369	8651	34603
0.64	14691	7787	33799
0.77	20380	5854	33054
0.90	26635	2908	32309

The relations (21a) and (21b) permit computing γ_i at any given P, T, and X_i using the equations:

$$RT\ln\gamma_{Cr_2O_3} = (2W_{G,Al_2O_3} - W_{G,Cr_2O_3})(1 - X_{Cr_2O_3})^2 + 2(W_{G,Cr_2O_3} - W_{G,Al_2O_3})(1 - X_{Cr_2O_3})^3 \quad (22a)$$

$$RT\ln\gamma_{Al_2O_3} = (2W_{G,Cr_2O_3} - W_{G,Al_2O_3})X^2_{Cr_2O_3} + 2(W_{G,Al_2O_3} - W_{G,Cr_2O_3})X^3_{Cr_2O_3}. \quad (22b)$$

And finally, equations (6) and (7) lead us to the activity (a_i) – composition (X_i) relations at high temperatures and pressures; two examples of such calculations are displayed in Figure 3. Note the significant positive deviation from ideality, which is consistent with both Jacob's and our calculated positive H_m^{ex} and negative S_m^{ex} values for the entire range of composition. Jacob's (1978, p. 175 and Fig. 2) claim that $a_{Al_2O_3}$ and $a_{Cr_2O_3}$ show both positive

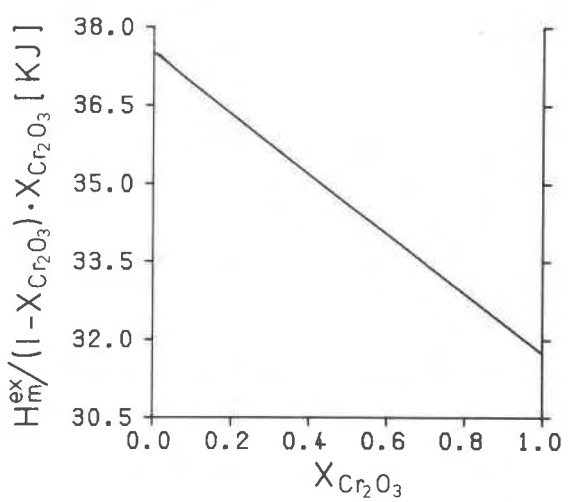

Fig. 2. $H_m^{ex}/(1 - X_{Cr_2O_3})\cdot X_{Cr_2O_3}$ *vs.* $X_{Cr_2O_3}$ diagram for P = 1 bar. The full line depicts 99 individual computations by us at intervals of 0.01 $X_{Cr_2O_3}$.

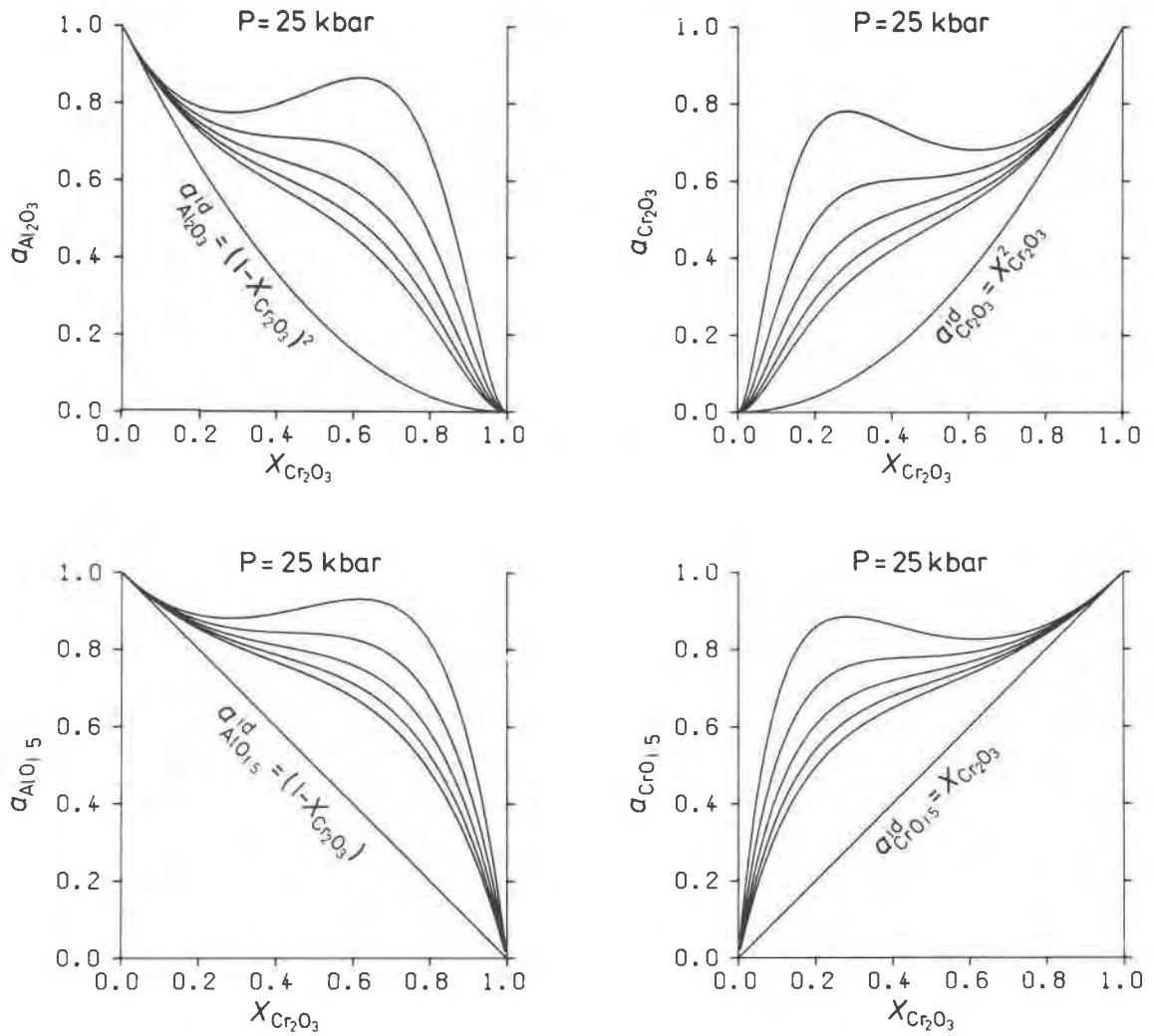

Fig. 3. Polythermal activity (a_i) *vs.* composition ($X_{Cr_2O_3}$) relation for α-$(Al,Cr)_2O_3$ crystalline solutions at P = 25 kbar, and for T = 800 (uppermost curve), 1000, 1200, 1400, and 1600° C (lowermost curve).

and negative deviations from Raoult's law stems from the fact that the *ideal activities* of the components Al_2O_3 and Cr_2O_3 are erroneously plotted as straight lines; compare Jacob's Figure 2 with Figure 3 of the present work.

The activity–composition data allow calculation of the solvus of corundum-eskolaite crystalline solutions. To achieve this, recall that both corundum solid solution, co, and eskolaite solid solution, es, obey the same equation of state, such that the conditions for their equilibrium coexistence on the solvus are:

$$a^{Co}_{Al_2O_3} = a^{Es}_{Al_2O_3} \tag{23a}$$

and

$$a^{Co}_{Cr_2O_3} = a^{Es}_{Cr_2O_3}. \tag{23b}$$

At any given P and T, the compositions of the coexisting phases require that the criteria for equilibrium (23a, 23b) be fulfilled simultaneously. Solution for compositions satisfying equations (23a) and (23b) was accomplished by iteration, following a method originally devised by Scatchard and revived recently by Luth and Fenn (1973). The isobaric spinodal curve was calculated by solving the relation (Thompson, 1967, eq. 90)

$$\begin{aligned}(\partial^2 G/\partial X^2_{Cr_2O_3})_{P,T} = 0 = {} & 2\,RT/(1 - X_{Cr_2O_3})\cdot X_{Cr_2O_3} \\ & + 2\,W_{G,Al_2O_3}(1 - 3X_{Cr_2O_3}) \\ & + 2\,W_{G,Cr_2O_3}(3X_{Cr_2O_3} - 2)\end{aligned} \tag{24}$$

for temperature, sweeping the composition sequen-

tially over the range $0 < X_{Cr_2O_3} < 1$. The critical constants T_c and X_c correspond to the maximum on the isobaric spinodal.

Figure 4 shows our calculated solvi and spinodals for the system Al_2O_3–Cr_2O_3 at 1 bar and 10, 30, and 50 kbar. At 1 bar, the critical composition was found to be 0.45 $X_{Cr_2O_3}$, which agrees very well with Jacob's (1978) calculations; however, the critical temperature is 945° C, rather than 900° C, as indicated by Jacob (1978, p. 178). At 50 kbar, $X_c = 0.44$ $X_{Cr_2O_3}$ and $T_c = 989°$ C, which indicates a pressure-dependence of the critical temperature $dT_c/dP = 0.88$ K/kbar. In other words, this solvus may be regarded as an excellent geothermometer. Of interest also is a comparison with previous attempts to determine the solvus directly by hydrothermal experiments (Neuhaus, 1963; Roy and Barks, 1972). Both of these studies are based on unreversed, short-duration hydrothermal runs. While Roy and Barks reported $T_c = 945°$ C and $X_c = 0.45$ $X_{Cr_2O_3}$ at 1 kbar, which is in excellent agreement with the present data, Neuhaus obtained a critical temperature near 800° C. However, a closer look at the two-phase data of Roy and Barks (1972, Fig. 1) reveals that their composition pairs agree remarkably well with our calculated spinodal at 1 bar, rather than with our solvus. It is tempting, therefore, to postulate that Roy and Barks (1972) determined the spinodal in their hydrothermal work.

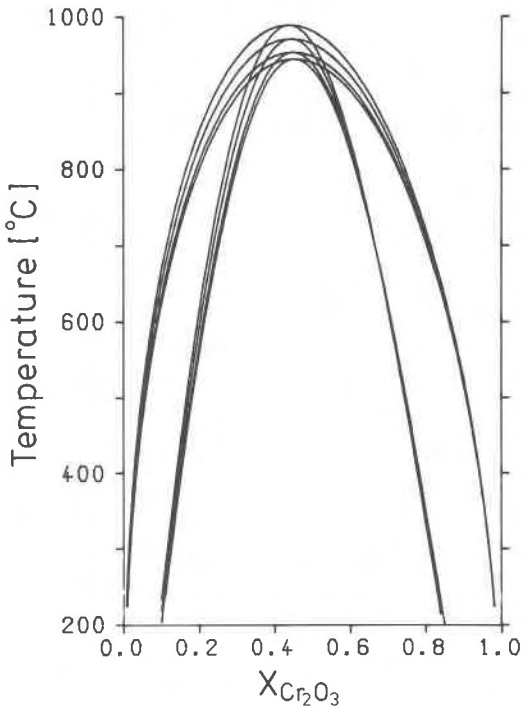

Fig. 4. Solvi and spinodals in the system Al_2O_3–Cr_2O_3 at $P = 1$ bar (bottom), 10, 30, and 50 kbar (top).

Geological applications

There are many potential applications of our knowledge of the thermodynamic mixing properties of corundum-eskolaite crystalline solutions. A few examples will be summarized here.

Chromian corundum—or ruby—is known to occur in various metamorphic rocks of low to medium grade. Examples of such assemblages are chromian corundum–margarite–anorthite (Okrusch *et al.*, 1976), chromian corundum–fuchsite–chromian andalusite–chromian diaspore, chromian corundum–fuchsite–chromian kyanite (Schreyer *et al.*, 1981). Due to lack of data on thermodynamic mixing properties of the various coexisting chromian phases, none of the possible $CrAl_{-1}$ exchange reactions or the net transfer reactions can be evaluated at present. More important, the conspicuous absence of the two-phase corundum–eskolaite assemblage can be readily explained as due to lack of proper bulk compositions. To our knowledge, the maximum Cr_2O_3-content reported to date does not exceed 2.5 mole % (Schreyer *et al.*, 1981). At a temperature of 400° C, where this corundum-bearing rock is believed to have equilibrated, the corundum solid solution will be expected to contain 3.4 mole % Cr_2O_3 component on the solvus. Evidently, lack of such two-phase assemblages in crustal rocks must be due to absence of requisite bulk compositions.

Corundum also occurs in many mantle-derived diamond-free or diamondiferous eclogites and grospydites. Although data on the chemical compositions of these corundums have been rarely reported, indications are that at least some of them are chromium-bearing (Sobolev, 1977; Carswell *et al.*, 1981). The most comprehensive chemical data available on such corundums are those from kimberlitic grosspydite xenoliths that occur in the Zagadochnaya pipe, Yakutia (Sobolev, 1977, Table 47). A wide range of miscibilities in the corundums is revealed, with Cr_2O_3 contents varying between 3 and 72 mole %, and Fe_2O_3 contents between 0.3 and 4.6 mole %. In one instance, textural evidence indicated fairly coarse exsolution blebs. Microprobe analyses yielded the compositions $(Al_{1.42}Cr_{0.55}Fe^{+3}_{0.02})_{1.99}O_3$ and $(Al_{0.72}Cr_{1.17}Fe^{+3}_{0.08})_{1.97}O_3$ for this phase-pair. If we choose to ignore the effect of minor Fe_2O_3 component and normalize the compositions to the join Al_2O_3–Cr_2O_3, these coexisting

phases correspond to a temperature of 910° C at a pressure of 30 kbar according to our calculated solvus. Clearly, the assemblage equilibrated to a rather low temperature prior to cessation of intercrystalline $CrAl_{-1}$ exchange. For a more rigorous interpretation of such natural two-phase assemblages, information on the ternary system Al_2O_3–Cr_2O_3–Fe_2O_3 is necessary. Experimental work (Turnock and Eugster, 1962) suggests very limited miscibility on the join Al_2O_3–Fe_2O_3, as do natural occurrences (Haslam *et al.*, 1980). The join Fe_2O_3–Cr_2O_3, however, is likely to exhibit extensive miscibility under geologic conditions.

Acknowledgments

We wish to thank Dr. W. Gebert for assistance with data collection on the Syntex R3 diffractometer, Drs. E. Froese and W. Maresch for critically reading an earlier version of the manuscript. Helpful editorial comments by Dr. J. G. Blencoe are appreciated. An anonymous editorial referee has been instrumental in our presenting the appendix. Financial support provided by the Deutsche Forschungsgemeinschaft, Bonn-Bad Godesberg, Germany under contracts Schr.64/36 and 64/37 is also gratefully acknowledged.

References

Abraham, K. and Schreyer, W. (1973) Elementverteilung in koexistierenden Festkörperphasen. Forschungsberichte des Landes Nordrhein-Westfalen, No. 2374, Westdeutscher Verlag, Opladen, Germany.

Appleman, D. E. and Evans, H. T. (1973) Job 9214: Indexing and least-squares refinement of powder diffraction data. U.S. Department of Commerce, National Technical Information Service, PB 216 188.

Bunting, E. N. (1931) Phase equilibria in the system Cr_2O_3–Al_2O_3. Journal of Research, National Bureau of Standards, 6, 947–949.

Carswell, D. A., Dawson, J. B., and Gibbs, F. G. F. (1981) Equilibrium conditions of upper mantle eclogites: implications for kyanite-bearing and diamondiferous varieties. Mineralogical Magazine, 44, 79–89.

Cassedanne, J. and Cassedanne, J. (1980) Présence d'eskolaite dans les alluvions stannifères de la Chapada Diamantina (Bahia-Brésil). Bulletin de Minéralogie, 103, 600–602.

Chiotti, P. (1972) New integration of the Gibbs-Duhem equation and thermodynamics of Pr–Zn alloys. Metallurgical Transactions, 3, 2911–2916.

Denbigh, K. (1971) The principles of chemical equilibrium. Cambridge University Press, Cambridge, England.

Freer, R. (1981) Interdiffusion studies in minerals with corundum structure: Al_2O_3–Cr_2O_3. In C. E. Ford, Ed., Progress in Experimental Petrology, p. 166–170. The Natural Environment Research Council Publication Series D18.

Graham, J. (1960) Lattice spacings and colour in the system alumina-chromic oxide. Journal of Physics and Chemistry of Solids, 17, 18–25.

Haslam, H. W., Brewer, M. S., Davis, A. E., and Darbyshire, D. P. F. (1980) Anatexis and high grade metamorphism in the Champira dome, Malawi: petrological and Rb–Sr studies. Mineralogical Magazine, 43, 701–714.

Jacob, K. T. (1978) Electrochemical determination of activities in Cr_2O_3–Al_2O_3 solid solution. Journal of the Electrochemical Society, 125, 175–179.

Kouvo, O. and Vuorelainen, Y. (1958) Eskolaite, a new chromium mineral. American Mineralogist, 43, 1098–1106.

Luth, W. C. and Fenn, P. M. (1973) Calculation of binary solvi with special reference to the sanidine-high albite solvus. American Mineralogist, 58, 1009–1015.

Moss, S. C. and Newham, R. E. (1964) The chromium position in ruby. Zeitschrift für Kristallographie, 120, 359–363.

Navrotsky, A. (1975) Thermochemistry of chromium compounds, especially oxides at high temperature. Geochimica et Cosmochimica Acta, 39, 819–832.

Neuhaus, A. (1963) Hydrothermal experiments on the miscibility of Al_2O_3–Cr_2O_3 at temperatures up to 800° C and pressures about 2000 atmospheres. The Physics and Chemistry of High Pressures (Ed.: Society of Chemical Industry, London), p. 237–239, Gordon and Breach Inc., New York.

Okrusch, M., Bunch, T. E., and Bank, H. (1976) Paragenesis and petrogenesis of a corundum-bearing marble at Hunza (Kashmir). Mineralium Deposita, 11, 278–297.

Roy, D. M. and Barks, R. E. (1972) Subsolidus phase equilibria in Al_2O_3–Cr_2O_3. Nature Physical Science, 235, 118–119.

Schreyer, W., Werding, G., and Abraham, K. (1981) Corundum-fuchsite rocks in greenstone belts of southern Africa: petrology, geochemistry and possible origin. Journal of Petrology, 22, 191–231.

Sobolev, N. V. (1977) Deep-seated inclusions in kimberlites and the problem of the composition of the upper mantle. (Translated from the Russian language by D. A. Brown). American Geophysical Union, Washington, D.C.

Steinwehr, H. E. v. (1967) Gitterkonstanten im System α-$(Al,Fe,Cr)_2O_3$ und ihr Abweichen von der Vegardregel. Zeitschrift für Kristallographie, 125, 377–403.

Thilo, E., Jander, J., and Seemann, H. (1955) Die Farbe des Rubins und der $(Al,Cr)_2O_3$-Mischkristalle. Zeitschrift für anorganische und allgemeine Chemie, 279, 2–17.

Thompson, J. B. (1967) Thermodynamic properties of simple solutions. In P. H. Abelson, Ed., Researches in Geochemistry, 2, 340–361. John Wiley, New York.

Turnock, A. C. and Eugster, H. P. (1962) Fe–Al oxides: phase relationships below 1000° C. Journal of Petrology, 3, 533–565.

Waldbaum, D. R. and Thompson, J. B. (1968) Mixing properties of sanidine crystalline solutions: II. Calculations based on volume data. American Mineralogist, 53, 2000–2017.

Manuscript received, June 3, 1981;
accepted for publication, February 19, 1982.

Appendix

The basic data on $\overline{G}^{ex}_{m,Cr_2O_3}$, $\overline{H}^{ex}_{m,Cr_2O_3}$, and $\overline{S}^{ex}_{m,Cr_2O_3}$ were obtained from Jacob (1978, Table 1), via equations (9), (10), and (11), respectively. Of these three quantities, only the uncertainty of $\overline{G}^{ex}_{m,Cr_2O_3}$ was given by Jacob, not, however, those for $\overline{H}^{ex}_{m,Cr_2O_3}$ and $\overline{S}^{ex}_{m,Cr_2O_3}$.

Two alternative procedures were followed for processing these data. The first method consisted of fitting the quantities $X_{Cr_2O_3}\cdot(\bar{G}^{ex}_{m,Cr_2O_3}/RT)$ and $X_{Cr_2O_3}\cdot\bar{H}^{ex}_{m,Cr_2O_3}$ to a polynomial in $X_{Cr_2O_3}$ having the form

$$X_{Cr_2O_3}\cdot\bar{Y}^{ex}_{m,Cr_2O_3} = a_1\cdot X_{Cr_2O_3} + a_2\cdot X^2_{Cr_2O_3} + a_3\cdot X^3_{Cr_2O_3} + a_4\cdot X^4_{Cr_2O_3} \quad (25)$$

subject to the four boundary constraints indicated in the text. Numerical integration of the Gibbs-Duhem equation followed the format of equation (16). Fitting $X_{Cr_2O_3}\cdot\bar{H}^{ex}_{m,Cr_2O_3}$ data was achieved using an optimization routine, minimizing the quantity

$$\sum_{i=1}^{7} |X_{Cr_2O_3}\cdot\bar{H}^{ex}_{m,Cr_2O_3,obs.} - X_{Cr_2O_3}\cdot\bar{H}^{ex}_{m,Cr_2O_3,calc.}|.$$

In obtaining a fit for $X_{Cr_2O_3}\cdot(\bar{G}^{ex}_{m,Cr_2O_3}/RT)$, an analogous procedure was followed, using the known uncertainties of $\bar{G}^{ex}_{m,Cr_2O_3}$ (Jacob, 1978, Table 1) at each composition as additional constraints. The value of $\bar{S}^{ex}_{m,Cr_2O_3}$ *vs.* $X_{Cr_2O_3}$ may be calculated from these. The averaged residuals of the fits are: $|\bar{H}^{ex}_{m,Cr_2O_3,obs.} - \bar{H}^{ex}_{m,Cr_2O_3,calc.}| = 6.1$ joules, $|\bar{S}^{ex}_{m,Cr_2O_3,obs.} - \bar{S}^{ex}_{m,Cr_2O_3,calc.}| = 0.163$ joule·Kelvin^{-1}, and $|\bar{G}^{ex}_{m,Cr_2O_3,obs.} - \bar{G}^{ex}_{m,Cr_2O_3,calc.}| = 207$ joules. The average uncertainty of our *derived* $\bar{G}^{ex}_{m,Cr_2O_3}$ may then be calculated from the residuals as 213.6 joules, which is well in accord with the average observed uncertainty for $\bar{G}^{ex}_{m,Cr_2O_3}$ of 287 joules. Nevertheless, the internal consistency, and thus, validity, of our derived thermodynamic data were questioned by an anonymous editorial referee, who indicated that the residuals for $|\bar{S}^{ex}_{m,Cr_2O_3,obs.} - \bar{S}^{ex}_{m,Cr_2O_3,calc.}|$ are probably too large. This prompted our devising the alternative method of data handling described below.

In the second method, all the three quantities—$X_{Cr_2O_3}\cdot(\bar{G}^{ex}_{m,Cr_2O_3}/RT)$, $X_{Cr_2O_3}\cdot\bar{H}^{ex}_{m,Cr_2O_3}$, and $X_{Cr_2O_3}\cdot\bar{S}^{ex}_{m,Cr_2O_3}$ – evaluable from Jacob's (1978) *emf* data, were fitted *simultaneously* to the above mentioned polynomial in $X_{Cr_2O_3}$ (equation (25)), subject to two constraints:

(i) the known uncertainty brackets of $\bar{G}^{ex}_{m,Cr_2O_3}$, and

(ii) $\bar{G}^{ex}_{m,Cr_2O_3} - \bar{H}^{ex}_{m,Cr_2O_3} + T\bar{S}^{ex}_{m,Cr_2O_3} = 0$ at each data point.

The latter constraint was necessary, because only two of the three $\bar{Y}^{ex}_{m,Cr_2O_3}$ values are independent. Data fitting by the optimization technique minimized the quantity

$$\left[\sum_{i=1}^{7} |X_{Cr_2O_3}\cdot\bar{H}^{ex}_{m,Cr_2O_3,obs.} - X_{Cr_2O_3}\cdot\bar{H}^{ex}_{m,Cr_2O_3,calc.}| + \sum_{i=1}^{7} |X_{Cr_2O_3}\cdot(\bar{G}^{ex}_{m,Cr_2O_3,obs.}/RT) - X_{Cr_2O_3}\cdot(\bar{G}^{ex}_{m,Cr_2O_3,calc.}/RT)| + \sum_{i=1}^{7} |X_{Cr_2O_3}\bar{S}^{ex}_{m,Cr_2O_3,obs.} - X_{Cr_2O_3}\cdot\bar{S}^{ex}_{m,Cr_2O_3,calc.}|\right]$$

Success of this method should establish that the $\bar{Y}^{ex}_{m,Cr_2O_3}$ values so derived are indeed thermodynamically consistent, because $\bar{G}^{ex}_{m,Cr_2O_3} - \bar{H}^{ex}_{m,Cr_2O_3} + T\bar{S}^{ex}_{m,Cr_2O_3}$ invariably vanishes at each data point; furthermore, all the derived quantities are also within the limits of uncertainty for $\bar{G}^{ex}_{m,Cr_2O_3}$ quoted by Jacob (1978). The residuals are: $|\bar{H}^{ex}_{m,Cr_2O_3,obs.} - \bar{H}^{ex}_{m,Cr_2O_3,calc.}| = 6.1$ joules, $|\bar{S}^{ex}_{m,Cr_2O_3,obs.} - \bar{S}^{ex}_{m,Cr_2O_3,calc.}| = 0.160$ joule·Kelvin^{-1}, and $|\bar{G}^{ex}_{m,Cr_2O_3,obs.} - \bar{G}^{ex}_{m,Cr_2O_3,calc.}| = 194$ joules. Further processing of these data leads to

$$W_{G,Cr_2O_3}\text{ (joules)} = 37484 + 0.0386\,P + 4.232\,T, \quad (21a')$$

and $W_{G,Al_2O_3}\text{ (joules)} = 31729 + 0.0006\,P + 4.838\,T, \quad (21b')$

which may be compared to the expressions for the same quantities (21a, 21b) obtained earlier by the first method. Calculation of the solvus based on (21a′) and (21b′) shows no change in X_c, while T_c turns out to be lower by *one* degree only at all values of pressure in the range 1 bar $\leqq P \leqq$ 50 000 bars.

Results given in the text follow our first method of data processing.